applied sciences

MDPI

Article

Parametric Optimization and Numerical Analysis of GaAs Inspired Highly Efficient I-Shaped Metamaterial Solar Absorber Design for Visible and Infrared Regions

Meshari Alsharari *, Ammar Armghan * and Khaled Aliqab

Department of Electrical Engineering, College of Engineering, Jouf University, Sakaka 72388, Saudi Arabia
* Correspondence: mmaalsharari@ju.edu.sa (M.A.); aarmghan@ju.edu.sa (A.A.)

Abstract: Renewable energy demand is increasing as fossil fuels are limited and pollute the environment. The solar absorber is an efficient renewable energy source that converts solar radiation into heat energy. We have proposed a gallium arsenide-backed solar absorber design made with a metamaterial resonator and SiO_2 substrate. The metamaterial resonator is investigated with thin wire metamaterial and I-shaped metamaterial designs. The I-shape metamaterial design outperforms the thin wire metamaterial design and gives 96% average absorption with a peak absorption of 99.95%. Structure optimization is applied in this research paper using parametric optimization. Nonlinear parametric optimization is used because of the nonlinear system results. The optimization method is used to optimize the design and improve the efficiency of the solar absorber. The gallium arsenide and silicon dioxide thicknesses are modified to see how they affect the absorption response of the solar absorber design. The optimized parameter values for SiO_2 and GaAs thicknesses are 2500 nm and 1000 nm, respectively. The effect of the change in angles is also investigated in this research. The absorption is high for such a wide angle of incidence. The angle of 30° only shows a lower absorption of about 30–50%. The effect of the change in angles is also investigated in this research. The design results are verified by presenting the E-field results for different wavelengths. The optimized solar absorber design applies to renewable energy applications.

Keywords: numerical; structure optimization; parametric optimization; metamaterial; renewable energy; solar absorber; absorption; gallium arsenide (GaAs)

Citation: Alsharari, M.; Armghan, A.; Aliqab, K. Parametric Optimization and Numerical Analysis of GaAs Inspired Highly Efficient I-Shaped Metamaterial Solar Absorber Design for Visible and Infrared Regions. *Appl. Sci.* **2023**, *13*, 2586. https://doi.org/10.3390/app13042586

Academic Editor: Wan Sharuzi Wan Harun

Received: 9 January 2023
Revised: 14 February 2023
Accepted: 15 February 2023
Published: 17 February 2023

1. Introduction

Renewable energy is energy collected from natural sources, and it provides pollution-free energy compared to fossil fuels [1]. Solar energy is a well-known renewable energy source because of its wide availability [2]. Solar energy can meet the high energy demands of today's world. The solar absorbers are designed to absorb the energy of solar radiation and convert it into heat, which can be used in different applications such as solar heaters, photovoltaic applications, etc. Solar absorbers are used to absorb not only visible energy but also ultraviolet and infrared energy to increase the overall efficiency of the absorber. The efficiency of the solar absorbers is also enhanced by optimizing the design using prediction algorithms [3]. Solar cells are another solar energy resource that convert solar radiation to electricity [4]. Solar cells should be efficient and low-cost to make energy affordable to all people. The solar absorber heat can also be converted into electricity, and in that way, solar absorbers can also be used to make effective and low-cost electricity [5,6]. The solar absorber can be made more effective by improving its absorption capacity, and this capacity can be improved by absorbing light from most of the solar spectrum. The broadband solar absorber is one of the options to improve efficiency. Broadband solar absorbers can be achieved by incorporating graphene and metamaterials in the absorber designs.

The graphene material can be incorporated into the solar absorber by placing its monolayer in the solar absorber design. The monolayer of graphene has the capacity to tune the spectrum to the far infrared spectrum, but in the solar absorber, there is a need to absorb more solar radiation. The incorporation of the graphene layer in the absorber makes it more absorbent because of the high conductivity and optical properties of graphene materials. Graphene-based solar absorbers absorb the energy from different regions and make it more effective. When graphene layers are placed over one another, they are used as a reflective surface as it reflects the light more, but when these graphene layers are wrinkled, a graphene ball sort of shape is formed, and then the reflection becomes very strong, and this design can be used for absorbing more light [7]. Reduced graphene oxide can be used in absorber design to improve its absorption. The coating of this graphene material on this solar absorber creates broadband absorption and increases the overall efficiency of the absorber design [8]. Graphene fabrication has also improved, and its use improves the efficiency of solar cells due to its unique properties [9]. Metamaterials are also added to the solar absorber design as a resonating element to improve its absorption [10]. Sometimes graphene and metamaterials are both added to improve their efficiency [11]. The graphene-based solar absorber is designed for improved absorption. Machine learning algorithms are used to improve absorption. The machine learning algorithm is used to optimize the different physical parameters. The optimization is also verified with the numerical simulation of the different physical parameters [12]. The new research work for parametric optimization, which improves the hyperparameters of machine learning algorithms, is presented. An evaluation of the algorithm is provided, with a special focus on two key features: the algorithm's efficiency when working with a subset of a dataset and its ability to complete the tuning process automatically, that is, without the user making explicit the number of iterations that the algorithm must perform [13]. Parametric optimization is also carried out to improve different mathematical operations using support vector machine parameters [14]. Graphene material is used in designing broadband solar absorbers, which are used for absorbing most of the visible spectrum and also some of the rest of the spectrum. There is a strong need for solar absorbers that not only absorb visible regions but also absorb other regions, which overall increases the solar absorber efficiency [15,16].

A metamaterial solar absorber is designed to be more absorbent based on silicon dielectric materials. The design gives high absorption with this metamaterial component in most of the visible region and some of the infrared region [17]. The metamaterial solar absorber is investigated numerically to achieve perfect absorption results. The structure is showing good absorption over most of the visible region [18]. The absorption of solar radiation is required for the whole day, and this can be achieved better with a wide angle of absorption for solar absorber design. One such solar absorber is designed in the visible region with good absorption for different angles of incidence [19]. Solar energy harvesting is done with a three-layer absorber for the visible region, with its high absorption available at two different frequencies [20]. Graphene and metamaterial-based absorbers can be designed to give multiband responses to be applicable in solar applications [12,21]. A perfect solar absorber is designed for the infrared spectrum using graphene material and metamaterials. The absorption spectra are also tuned to different frequencies in the near-infrared spectrum [22]. The metamaterial absorber uses a metamaterial component as a resonator, which improves the absorption of the solar absorber design [23]. Metamaterials are sometimes combined with graphene material to absorb solar energy and generate highly efficient solar absorbers [24]. Zirconium nitride is combined with metamaterials and graphene to improve solar absorber absorption in the visible and infrared spectrums [25].

The optimization of the parameters is required to improve the system's performance. In this research, the parameters are improved using parametric optimization with a nonlinear parametric optimization algorithm. Nonlinear optimization is utilized in situations in which the function does not behave linearly in relation to the variable being optimized for. Nonlinear optimization is having a function $f(x)$, or a constraint $c_i(x) = 1, 2, \ldots n$ or $d_j(x) = 0, 1, \ldots n$, are nonlinear functions of the vector of variables x [26]. Broadband absorbers absorb the majority of the energy in the visible spectrum, as discussed in the literature, and only a portion of the energy in other regions is absorbed, so there is a need for an absorber that absorbs energy from most of the spectrums. We have proposed an absorber that absorbs solar radiation in the visible and infrared spectra. Thus, the efficiency of the solar absorber is increasing. The absorber is designed on a two-layer substrate with a metamaterial resonator. The metamaterial resonator is also placed over the graphene monolayer to improve the overall absorption. The following sections discuss the design and the results of the design.

2. Numerical Analysis

This section shows the design and development of the solar absorber. The solar absorber development is done using three layers in this design. The two substrate layers, namely SiO_2 and GaAs, are used. The selection of these substrates is done because of their wide availability for the solar absorber design and their absorbing capacity. The resonating layer is made up of titanium material. Titanium is a low-cost material compared to gold and silver. This low-cost behavior of this metal will improve its affordability for different classes of people. Figure 1 depicts the three-layer design, including the graphene layer as a sandwiching layer between the resonator and SiO_2 substrate. The optimization of the structural parameters has been investigated in this design, and the optimized parameters for different parameters are 1000 nm for the I-shaped resonator thickness, 1000 nm for the GaAs substrate, and 2500 nm for the SiO_2 substrate. There is no ground plane used in this design. Optimization of I-shape design parameters such as length, width, and edges is also performed. The two different metasurface designs, such as the I-shape design and the thin wire design, are also carried out, and their results are presented in the next section. The length and width of the substrate are 7000 nm and 7000 nm, respectively. I-shape length and width are 3000 nm and 3000 nm, respectively. The thin wire's length and width are 3000 nm and 500 nm, respectively.

The graphene material is very important in the design of this absorber because it enhances the absorptance of the solar design by incorporating a monolayer of it between the resonator and substrate. The optical and electric properties are helping to improve the overall efficiency of the design. The change in graphene's chemical potential changes the conductivity of the monolayer, which will improve the absorption of the structure. The equation for these is presented in Equations (1)–(4) [27]. The absorption also depends on the angle of incidence, which is presented in Equations (5)–(11) [28]

$$\varepsilon(\omega) = 1 + \frac{\sigma_s}{\varepsilon_0 \omega \Delta} \tag{1}$$

$$\sigma_{intra} = \frac{-je^2 k_B T}{\pi\hbar^2(\omega - j2\Gamma)}\left(\frac{\mu_c}{k_B T} + 2ln\left(e^{-\frac{\mu_c}{k_B T}} + 1\right)\right) \tag{2}$$

$$\sigma_{inter} = \frac{-je^2}{4\pi\hbar} ln\left(\frac{2|\mu_c| - (\omega - j2\Gamma)\hbar}{2|\mu_c| + (\omega - j2\Gamma)\hbar}\right) \tag{3}$$

$$\sigma_s = \sigma_{inter} + \sigma_{intra} \tag{4}$$

The angle of incidence and absorption relation

$$r(\omega, \theta_i) = \frac{\omega \cos\theta_i \prod_{00}(\omega, \theta_i)}{2i\hbar c k^2 + \omega \cos\theta_i \prod_{00}(\omega, \theta_i)} \tag{5}$$

$$\sigma_{||}(\omega, k) = -i\,\frac{\omega}{4\pi\hbar k^2} \prod_{00}(\omega, k) \tag{6}$$

$$r(\omega, \theta_i) = \frac{2\pi \cos\theta_i \sigma_{||}(\omega, k)}{c + 2\pi \cos\theta_i \sigma_{||}(\omega, k)} \tag{7}$$

$$\mathcal{R}(\omega, \theta_i) = |r(\omega, \theta_i)|^2 \tag{8}$$

$$\mathcal{R}(\omega,\theta_i) = \frac{4\pi^2\cos^2\theta_i\left[\mathrm{Re}^2\sigma_{||}(\omega,k) + \mathrm{Im}^2\sigma_{||}(\omega,k)\right]}{\left[c + 2\pi\cos\theta_i\mathrm{Re}\sigma_{||}(\omega,k)\right]^2 + 4\pi^2\cos^2\theta_i\mathrm{Im}^2\sigma_{||}(\omega,k)} \tag{9}$$

$$\mathcal{R}(\omega) = \mathcal{R}(\omega,0) = \frac{4\pi^2\left[\mathrm{Re}^2\sigma(\omega) + \mathrm{Im}^2\sigma(\omega)\right]}{[c + 2\pi\mathrm{Re}\sigma(\omega)]^2 + 4\pi^2\mathrm{Im}^2\sigma(\omega)} \tag{10}$$

$$A(\omega) = 1 - \mathcal{R}(\omega) - T(\omega) \tag{11}$$

The results of all these analyses related to optimization are discussed in the following sections.

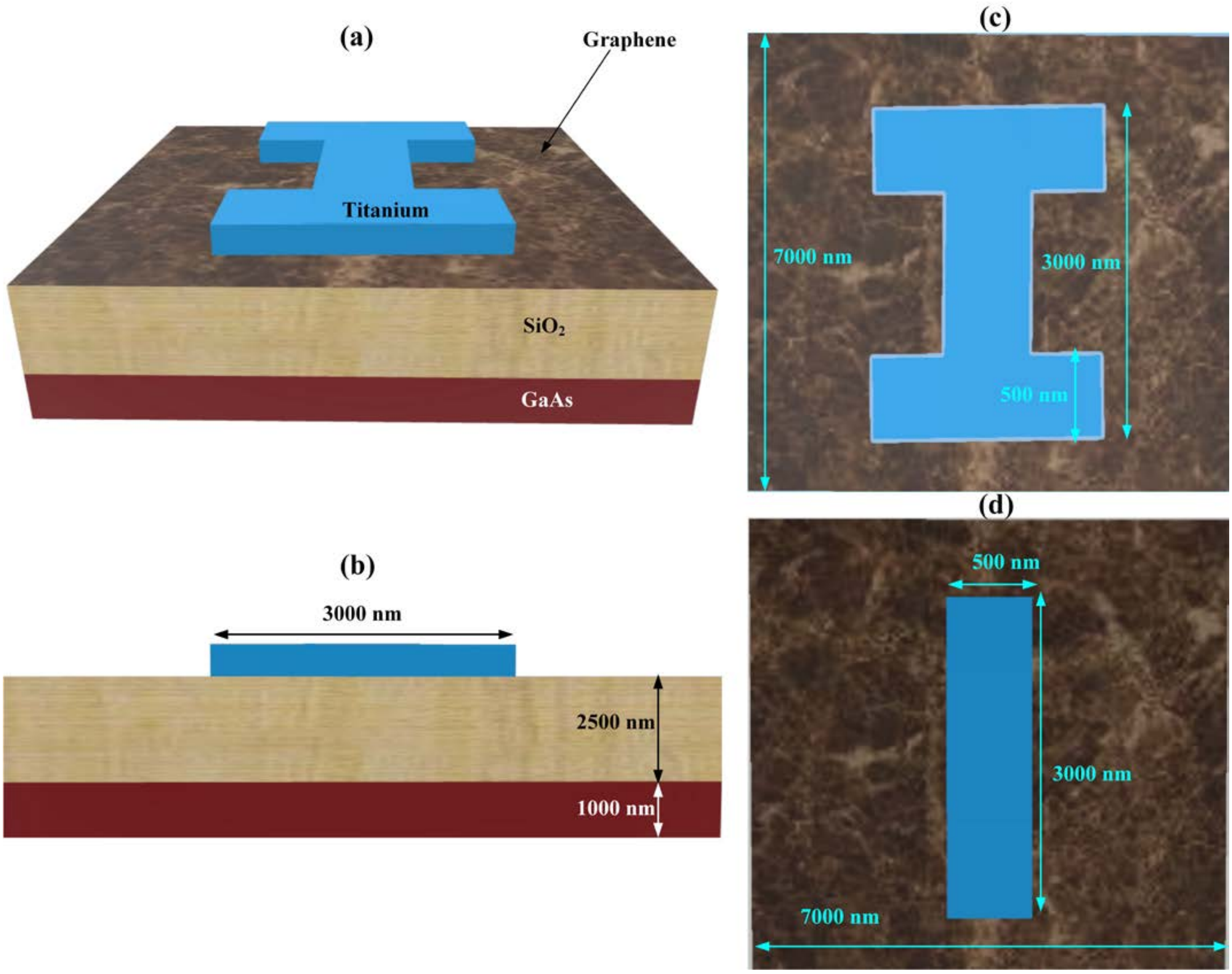

Figure 1. Structural design of the I-shaped and thin wire metasurface solar absorber. (**a**) an I-shaped solar absorber 3D view; (**b**) an I-shaped metasurface solar absorber front view; (**c**) an I-shaped metasurface solar absorber top view; (**d**) a thin wire metasurface solar absorber top view. The size of different parameters is presented in the figure. The length, width, and height of the substrate are 7000 nm, 7000 nm, and 2500 nm, respectively. The I shape and thin wire length are 3000 nm. The total length and width of an I-shape are both 3000 nm. A thin wire has dimensions of 3000 nm in length and 500 nm in width. The figure is not up to the scale. The three-layer design with sandwiching graphene layers is visible in the figure.

3. Analysis of Results

The investigation of the I-shaped design and thin wire design is analyzed using COMSOL Multiphysics. The simulation is done based on the FEM. The result for the I-shaped design and thin wire design is presented for the range of 500 nm to 3000 nm.

The wavelength band presented includes the wavelengths of the visible and infrared regions. The absorption results for these two designs are also compared in Figure 2a,b. In Figure 2b, the numerical values of the responses are presented for the average absorption, and they are compared. The I-shape metamaterial design results show an overall average absorption of 96% for the whole range, while the thin wire design shows a 95% result for the same range, which clearly shows that the I-shape metamaterial is giving optimum performance compared to the thin wire design of the metasurface-based solar absorber design. The absorption results in Figure 2 show that there are about five peaks near the perfect absorption achieved. The absorption level for this absorption peak is more than 99%, with the highest peak having an absorption of 99.5%. Thus, this proposed solar absorber is also showing perfect absorption behavior. The response in the figure shows that in the initial phase, the absorption curve is the same, but after 1500 nm, the absorption of the I-shape metamaterial design is higher compared to the thin wire metamaterial design. The change in response is achieved because of the metasurface shape, which was converted from a thin wire shape to an I-shape. The I-shape has more area compared to the thin wire shape. The increase in area increases the overall inductance, which will result in more absorption compared to the thin shape. The I-shape design is further investigated for optimal geometrical parameters. The optimization is carried out for various dimensions of the substrate and resonator. The result of this structure optimization is discussed in the following section.

(a)

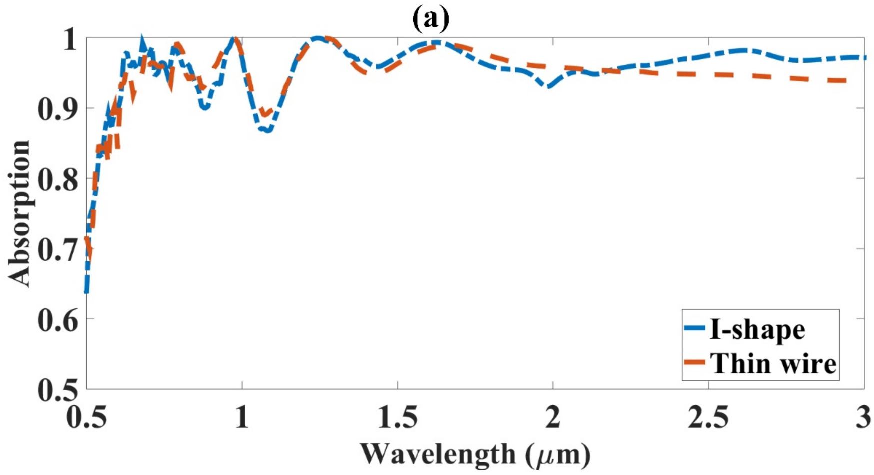

(b)

Design	Average Absorption (%)
I- shape design	96
Thin wire design	95

Figure 2. The metamaterial design comparative response for I-shape design and thin wire design is shown in (**a**) an absorption plot (**b**) and a comparative table with numerical data. The highest average absorption response is 96% for the I-shape metamaterial design.

The electric field response of the I-shape design is studied to verify its effect on the absorption results. The absorption results of the I-shape design presented in Figure 2 can be verified by the amount of electric energy concentrated in the solar absorber, which is presented in the electric field response figure. The E-field response is investigated in Figure 3. The electric field response is presented for six different points on the wavelength spectrum. These six different wavelength points of the spectrum are identified based on the different absorption levels at those points, allowing the field energy to be explored at those different wavelength points. The different wavelength points that are investigated here are 500 nm, 1000 nm, 1500 nm, 2000 nm, 2500 nm, and 3000 nm. The six points cover the whole spectrum of wavelengths observed for absorption results. The E-field response presents that as the wavelength of investigation is increased, the absorption is also increased, and the absorption is also achieved through SiO_2 and GaAs substrates. Thus, it can be concluded that the GaAs substrate-backed solar absorber is performing well in the infrared region, which is visible in this electric field response. The highest E-field of 2.5×10^6 is visible in the response presented in Figure 3. The E-field response presented in the figure shows good field distribution in the metamaterial resonator and substrate. The substrate is also visible in the figure, with a high-field red color response. The result also verified the responses presented in Figure 2 for different wavelengths. The different colors and related fields are also presented in the figure, with the field response inset presented on the right side of the figure.

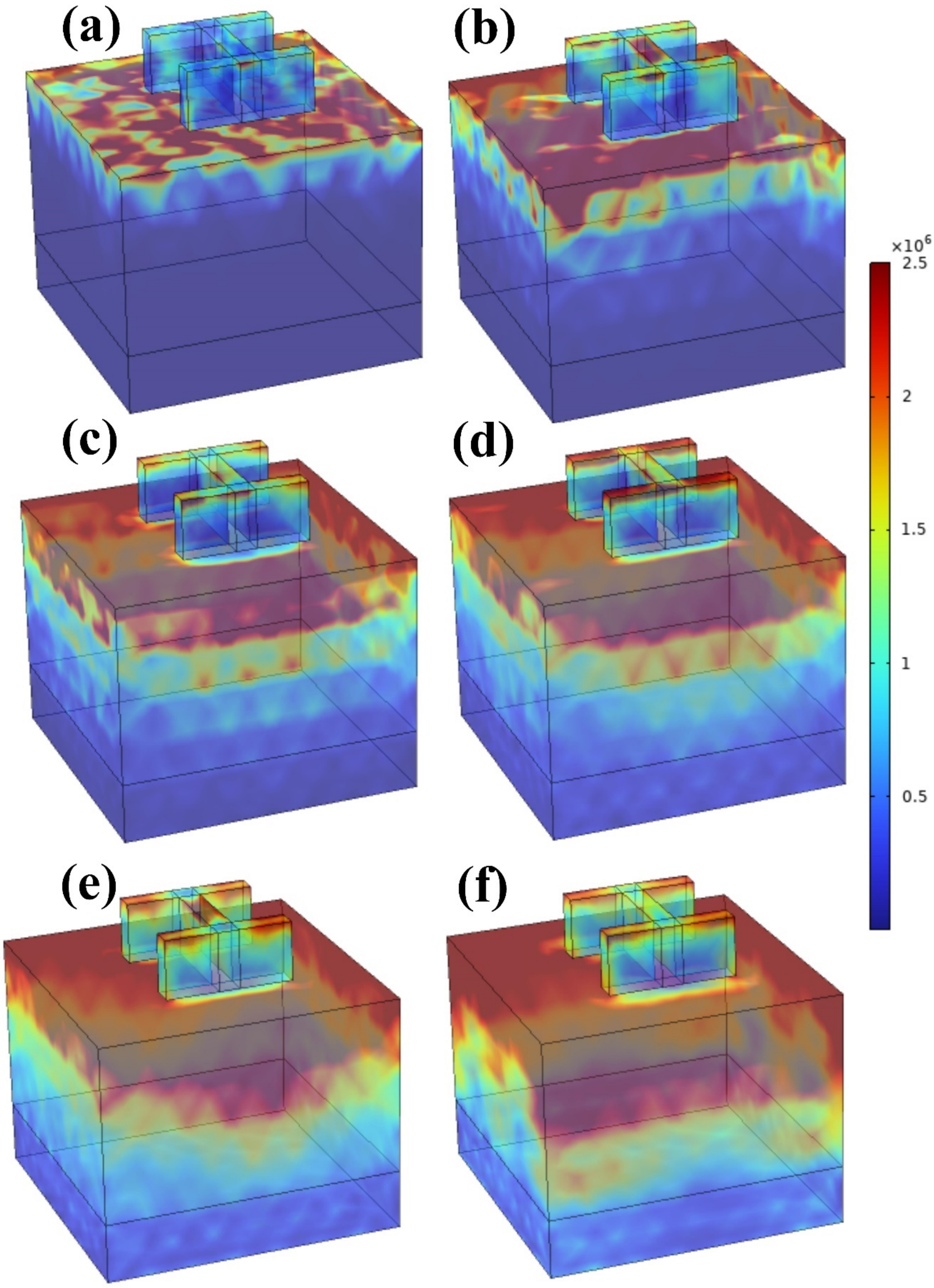

Figure 3. E-field results for the I-shaped metamaterial design backed by gallium arsenide at (**a**) 500 nm, (**b**) 1000 nm, (**c**) 1500 nm, (**d**) 2000 nm, (**e**) 2500 nm, and (**f**) 3000 nm. The color bar shows the electric field values, which are at their highest value of 2.5×10^6 V/m.

The E-field response at 500 nm shown in Figure 3a demonstrates that the electric field is visible at the substrate's surface and in the metasurface. The level of the E-field is low. This electric field response matches the absorption response available at 500 nm, which is around 60%. The E-field response shown in Figure 3b for 1000 nm shows that the electric field is visible not only at the surface like the previous response, but it is also visible going into the substrate a little bit. The E-field response at 1500 nm shown in Figure 3c indicates that the electric field is visible throughout the substrate, with higher energy on the upper part of the substrate and lower energy on the lower part of the substrate. The E-field response at 2000 nm shown in Figure 3d indicates that the electric field is visible throughout the substrate, with higher energy on the upper and middle surfaces and lower energy on the bottom surface. The E-field response shown in Figure 3e for 2500 nm shows that the electric field is visible in the whole substrate, with higher energy on the upper, middle, and lower parts of the substrate, with energy also visible in the second substrate below the SiO_2 substrate. The E-field response shown in Figure 3f for 3000 nm shows that the electric field is visible in the whole SiO_2 substrate, and some part of the energy is also visible in the second substrate of GaAs. This electric field response matches well with the absorption response available at 3000 nm shown in Figure 1, which is more than 96%.

4. Structural Optimization

The structure optimization is carried out to optimize the absorption of the solar absorber design. There are different methods to optimize the structure. One of the important methods is parametric optimization. Parametric optimization is used to optimize the results while keeping the different constraints in consideration. The behavior of the system is nonlinear, so nonlinear optimization algorithms can be used to optimize the different parameters. In this section, we have detailed the optimization method and also presented the optimized results using numerical investigation.

The optimization of the structure is generally done with different types of optimization. One of the important optimizations is parametric optimization. We have explained the parametric optimization here in detail before we present the structure optimization results. Parametric optimization is one of the important methods to optimize the results of the solar absorber design [29]. Nonlinear optimization is utilized in situations in which the function does not behave linearly in relation to the variable being optimized for. Nonlinear optimization is having function f(x), or constraint $c_i(x) = 1, 2, \ldots n$ or $d_j(x) = 0, 1, \ldots n$, are nonlinear functions of the vector of variables x. Several researchers make use of the nonlinear optimization method in order to enhance the results obtained from the nonlinear system [30]. The gradient nonlinear optimization method is also one of the useful methods for determining the maximal nonlinear systems for energy conversion [31].

In our research, we have used a nonlinear optimization algorithm as our research shows nonlinear behavior. The absorption is the result that needs to be maximized, while the parameter that needs to be optimized has different physical and geometrical parameters. The research is also using wavelength to observe the maximum absorption while varying the different geometrical parameters. The results related to the optimization are presented in Figures 4 and 5 and discussed in detail in this section. The degree of influence of the optimization algorithm is also discussed in this section.

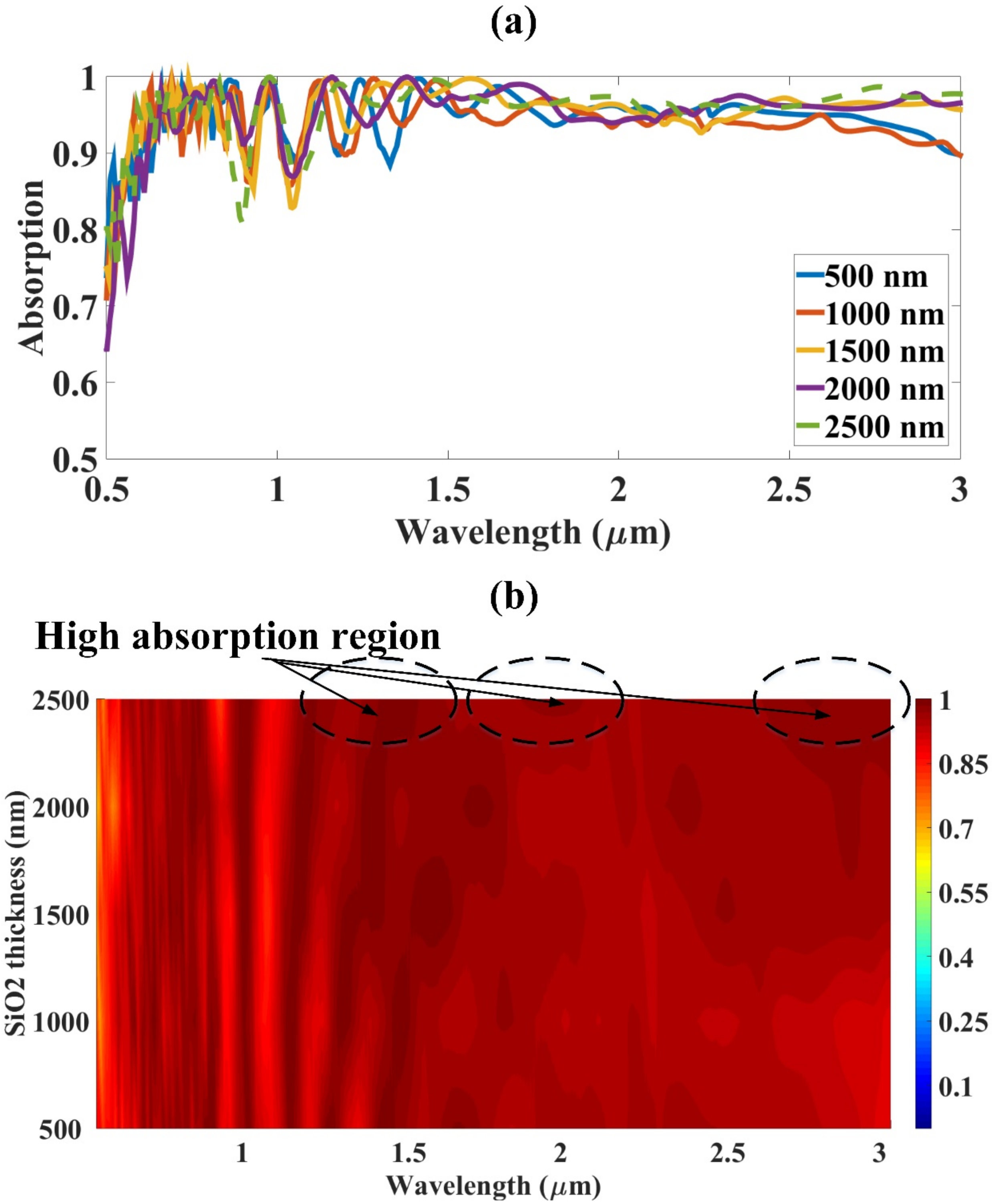

Figure 4. The impact of SiO_2 thickness change on absorption is shown in (**a**) the absorption response for 500 nm to 2500 nm SiO_2 thickness variation in a line plot and (**b**) the absorption response for 500 nm to 2500 nm variation in a color plot, with red having the highest absorption. The high absorption regions are marked in circles at 2500 nm. The high absorption is also visible in the line plot, with the green color line having a 2500 nm value.

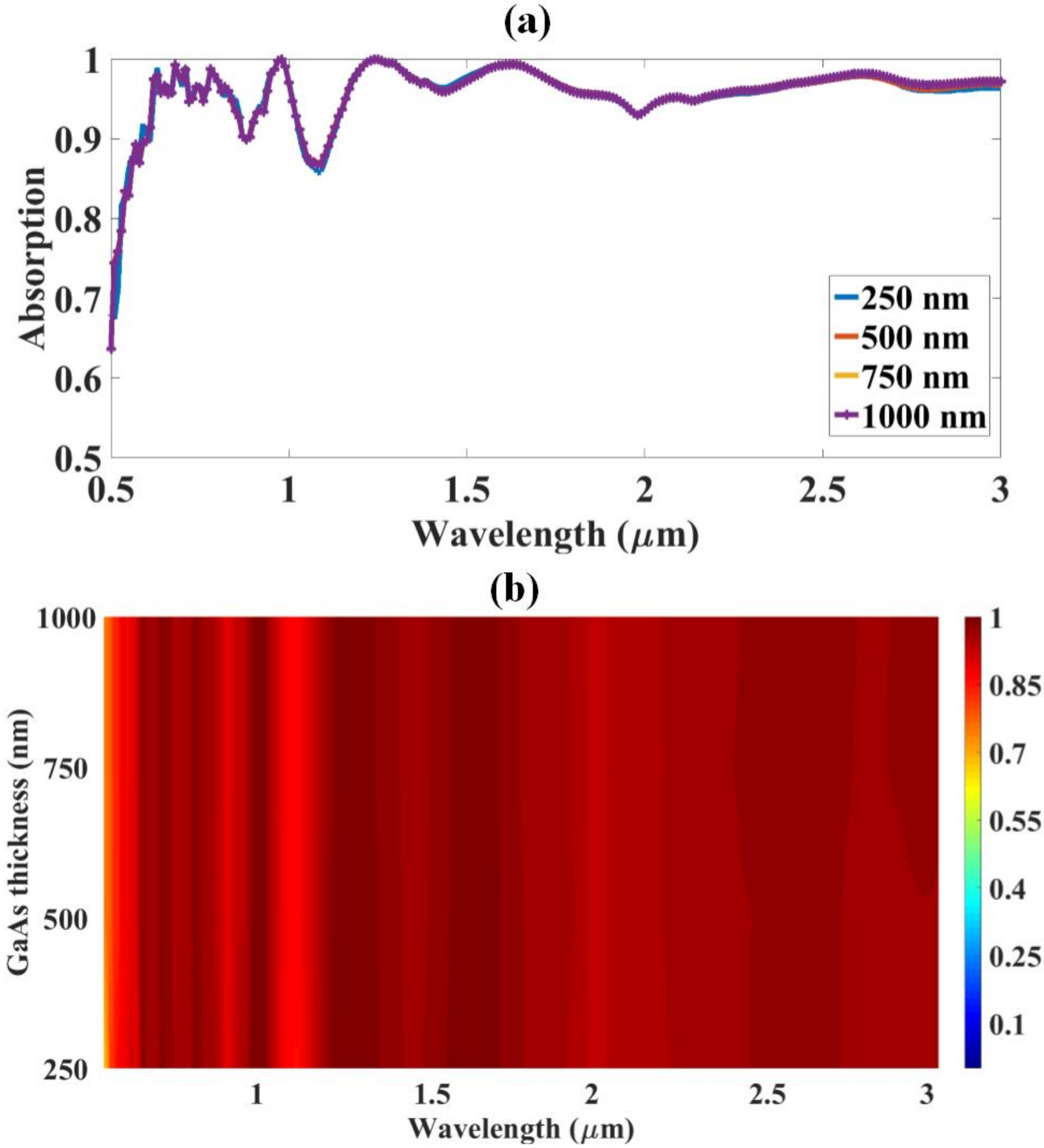

Figure 5. The impact of GaAs thickness change on absorption is shown in (**a**) the absorption response for 250 nm to 1000 nm GaAs thickness variation in a line plot and (**b**) the absorption response for 250 nm to 1000 nm variation in a color plot, with the red color having the highest absorption. The absorption is nearly constant across the entire range of GaAs material thickness variations.

The structural optimization is carried out on the two dielectric materials used as substrates in this design. First, the SiO_2 substrate height is varied from 500 nm to 2500 nm. The response to this change is investigated in Figure 4. The result shows that the highest thickness of 2500 nm has more absorption compared to the other thicknesses. The absorption is higher in this thickness because of the higher area provided for the absorption of the signal. The red part of Figure 4b, marked with circles, shows the high absorption regions in the 2500 nm thickness range. The line plot also shows that high absorption for this thickness is available at three different locations, as presented in the color plot. The increase in further thickness is not checked because the higher thickness is making the area and size of the structure large as well as increasing the inductance, which affects the results. Instead of increasing the thickness further in the same material, we have added GaAs material at the back of this solar absorber, which has a different refractive index and also helps in gaining further absorption. The results for GaAs thickness change are given in Figure 5. The bottom layer added to the substrate is increasing the absorption slightly because of the difference in refractive indices between the two materials. The variation in thickness of this material is not affecting the absorption further, and the same is visible in Figure 5. The absorption level around 1 m shows perfect absorption, with 99.5% absorption as the result. The absorption levels are in three peaks, with the highest having perfect absorption with more than 99% absorption. The results are also showing a similar performance for all the variations in GaAs thickness. The results of the optimization clearly show that there is an increase in absorption with increasing substrate thickness. The thickness improvement also shows that nonlinear parametric optimization is essential and that there is an increase in absorption for higher thicknesses. The increased thickness is the key to improving absorption. The increased thickness influences the overall efficiency of the solar absorber design. The thickness increase was kept to a limit to keep the design complexity and cost lower.

The angle of incidence variation is observed by varying the different angles of incidence from 0 degrees to 80 degrees. The angle of incidence is varied to observe its effect on the results. The angle of incidence variation is not affecting the results much, as presented in Figure 6. The result clearly shows that absorption is high for most of the angles except the 30° angle. The blue color shows the reduction in absorption for an angle range between 30° and 80°. The red color around other angles indicates high absorption of the red color. The results show that the absorption is high for most of the angles of incidence. The angle at which the absorption is less is also important. The absorption for different angles clearly shows that the solar absorber is giving better results for most of them. The low angles are also showing 30–50% absorption, which is good for solar absorbers as it is going to increase the absorption of the solar absorber.

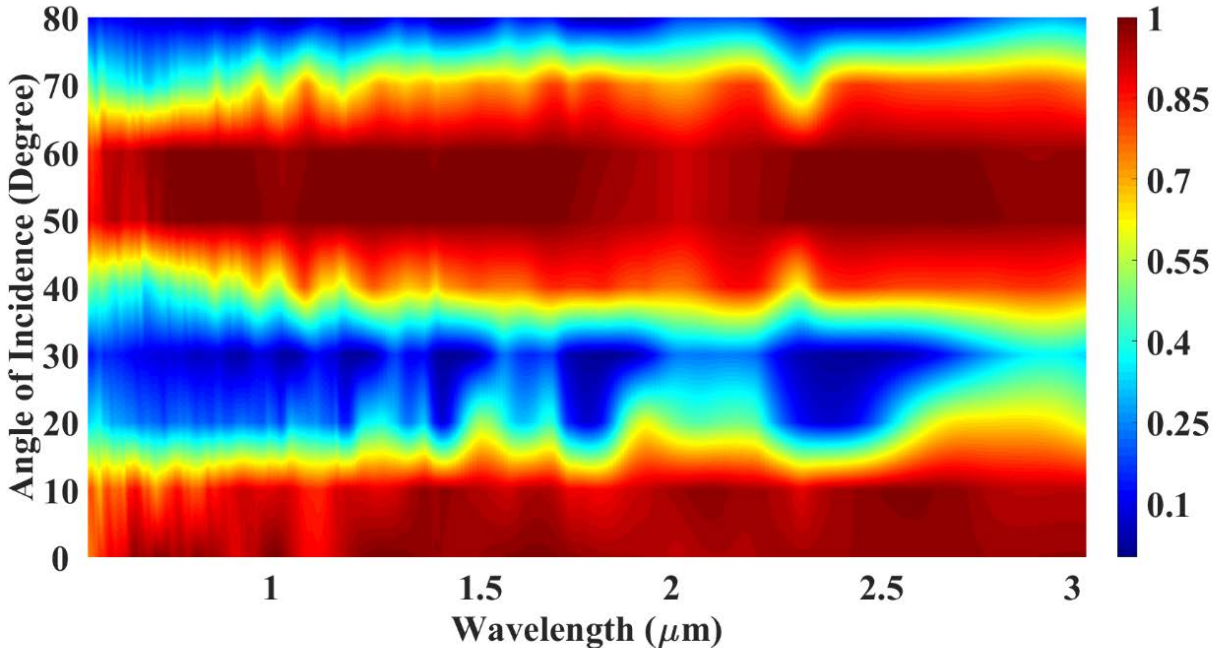

Figure 6. Angle of incidence variation for wavelengths from 500 nm to 3000 nm. For most of the range, absorption is high. The 30° does not have high absorption until 2500 nm, after which absorption improves until 3000 nm. The absorption level is good for most of the angles. The 30° angle angle exhibits 30–50% absorption.

The comparison of the I-shaped metamaterial design is observed in Table 1. The I-shaped metamaterial design is showing 96% average absorption in the visible and infrared regions. This absorption is higher compared to the rest of the references presented in the table. The absorption results show that the I-shape metamaterial design is showing the maximum absorption. The comparison of the proposed I-shape metamaterial design with other published designs shows its improvement in terms of the absorption of the solar absorber. There is one published design with 95% average absorption, but it gives absorption in a lower wavelength range compared to our proposed design results, which give results in the wide wavelength range of 500 nm to 3000 nm.

Table 1. Comparison of solar absorber designs with the proposed double substrate design of I-shape metamaterial and thin metamaterial.

Design	Visible and Infrared Region from 500 nm to 3000 nm	Cost (Unit Cell)
I-shape metamaterial design	96	Low
Thin wire metamaterial design	95	Low
[32]	90	Moderate
[33]	90	Moderate
[34]	86.5	Low
[35]	93	High
[36]	93.1	Low
[37]	90	High
[38]	95	Low
[39]	80	High
[40]	71.1	High
[21]	70	High
[41]	84	Low
[42]	93.7	Moderate
[43]	92	High

5. Conclusions

The need for renewable and clean energy has opened the way for designing highly efficient solar absorbers. One such solar absorber is designed with an I-shaped metamaterial resonator backed by SiO_2 and GaAs substrates. The I-shaped metamaterial design is also compared with the thin-wire metamaterial design to obtain the optimized metamaterial design. The I-shaped metamaterial has the highest absorption, at 96%, in the 500 nm to 3000 nm wavelength range. It is also showing a peak absorption of 99.95% in the infrared range. The I-shaped optimized design is also investigated for E-field response, which clearly shows that for higher wavelengths absorption is higher because of the GaAs substrate. The optimization of the structure is also investigated for SiO_2 and GaAs thicknesses. The effect of GaAs thickness is minimal, and it is visible at higher wavelengths. A perfectly designed solar absorber can be used for solar thermal energy conversion applications. Further improvement in the absorption can be achieved in the future by changing the materials and applying the other metamaterial component in the design.

Author Contributions: conceptualization, M.A. and A.A.; methodology, K.A.; software, M.A. and A.A.; validation, M.A.; formal analysis, A.A. and K.A.; investigation, M.A. and A.A.; resources, M.A. and A.A.; writing—original draft preparation, all authors; writing—review and editing, all authors. All authors have read and agreed to the published version of the manuscript.

Funding: The authors extend their appreciation to the Deputyship for Research and Innovation, Ministry of Education in Saudi Arabia, for funding this research work through the project number 223202.

Data Availability Statement: The data will be made available at the corresponding author's reasonable request.

Conflicts of Interest: The authors declare no conflict of interest.

References

1. Clausen, L.T.; Rudolph, D. Renewable energy for sustainable rural development: Synergies and mismatches. *Energy Policy* **2020**, *138*, 111289. [CrossRef]
2. AL-Rjoub, A.; Rebouta, L.; Costa, P.; Barradas, N.; Alves, E.; Ferreira, P.; Abderrafi, K.; Matilainen, A.; Pischow, K. A design of selective solar absorber for high temperature applications. *Sol. Energy* **2018**, *172*, 177–183. [CrossRef]
3. Parmar, J.; Patel, S.K.; Katkar, V. Graphene-based metasurface solar absorber design with absorption prediction using machine learning. *Sci. Rep.* **2022**, *12*, 2609. [CrossRef] [PubMed]
4. Kumavat, P.P.; Sonar, P.; Dalal, D.S. An overview on basics of organic and dye sensitized solar cells, their mechanism and recent improvements. *Renew. Sustain. Energy Rev.* **2017**, *78*, 1262–1287. [CrossRef]
5. Jiang, Q.; Zhao, Y.; Zhang, X.; Yang, X.; Chen, Y.; Chu, Z.; Ye, Q.; Li, X.; Yin, Z.; You, J. Surface passivation of perovskite film for efficient solar cells. *Nat. Photonics* **2019**, *13*, 460–466. [CrossRef]
6. Parmar, J.; Patel, S.K.; Katrodiya, D.; Nguyen, T.K.; Skibina, J.S.; Dhasarathan, V. Numerical investigation of gold metasurface based broadband near-infrared and near-visible solar absorber. *Phys. B Condens. Matter* **2020**, *591*, 412248. [CrossRef]
7. Hao, W.; Chiou, K.; Qiao, Y.; Liu, Y.; Song, C.; Deng, T.; Huang, J. Crumpled graphene ball-based broadband solar absorbers. *Nanoscale* **2018**, *10*, 6306–6312. [CrossRef] [PubMed]
8. Thakur, A.K.; Sathyamurthy, R.; Sharshir, S.W.; Kabeel, A.E.; Elkadeem, M.; Ma, Z.; Manokar, A.M.; Arıcı, M.; Pandey, A.; Saidur, R. Performance analysis of a modified solar still using reduced graphene oxide coated absorber plate with activated carbon pellet. *Sustain. Energy Technol. Assess.* **2021**, *45*, 101046. [CrossRef]
9. Shi, Z.; Jayatissa, A.H. The impact of graphene on the fabrication of thin film solar cells: Current status and future prospects. *Materials* **2017**, *1*, 36. [CrossRef]
10. Patel, S.K.; Parmar, J.; Katrodiya, D.; Nguyen, T.K.; Holdengreber, E.; Dhasarathan, V. Broadband Metamaterial-based Near-infrared Absorber using Array of Uniformly Placed Gold Resonators. *J. Opt. Soc. Am. B* **2020**, *37*, 2163–2170. [CrossRef]
11. Patel, S.K.; Surve, J.; Jadeja, R.; Katkar, V.; Parmar, J.; Ahmed, K. Ultra-wideband, polarization-independent, wide-angle multilayer Swastika-shaped metamaterial solar energy absorber with absorption prediction using machine learning. *Adv. Theory Simul.* **2022**, *5*, 2100604. [CrossRef]
12. Patel, S.K.; Parmar, J.; Katkar, V. Graphene-based multilayer metasurface solar absorber with parameter optimization and behavior prediction using Long Short-Term Memory model. *Renew. Energy* **2022**, *191*, 7–58. [CrossRef]
13. Castañeda, Á.L.M.; Decastro-García, N.; García, D.E. Rhoaso: An early stop hyper-parameter optimization algorithm. *Mathematics* **2021**, *9*, 2334. [CrossRef]
14. Fang, H.; Fu, X.; Zeng, Z.; Zhong, K.; Liu, S. An Improved Arithmetic Optimization Algorithm and Its Application to Determine the Parameters of Support Vector Machine. *Mathematics* **2022**, *10*, 2875. [CrossRef]
15. Patel, S.K.; Parmar, J.; Katkar, V. Metasurface-based solar absorber with absorption prediction using machine learning. *Opt. Mater.* **2022**, *124*, 112049. [CrossRef]
16. Charola, S.; Patel, S.K.; Parmar, J.; Ladumor, M.; Dhasarathan, V. Broadband graphene-based metasurface solar absorber. *Microw. Opt. Technol. Lett.* **2020**, *62*, 1366–1373. [CrossRef]
17. Obaidullah, M.; Esat, V.; Sabah, C. Multi-band (9,4) chiral single-walled carbon nanotube based metamaterial absorber for solar cells. *Opt. Laser Technol.* **2021**, *134*, 106623. [CrossRef]
18. Bagmanci, M.; Karaaslan, M.; Unal, E.; Akgol, O.; Baklr, M.; Sabah, C. Solar energy harvesting with ultra-broadband metamaterial absorber. *Int. J. Mod. Phys. B* **2019**, *33*, 1950056. [CrossRef]
19. Shuvo, M.M.K.; Hossain, M.I.; Rahman, S.; Mahmud, S.; Islam, S.S.; Islam, M.T. A Wide-Angle, Enhanced Oblique Incidence, Bend-Able Metamaterial Absorber Employed in Visible Region with a Sun Shape Resonator. *IEEE Access* **2021**, *9*, 126466–126480. [CrossRef]
20. Mulla, B.; Sabah, C. Multiband Metamaterial Absorber Design Based on Plasmonic Resonances for Solar Energy Harvesting. *Plasmonics* **2016**, *11*, 1313–1321. [CrossRef]
21. Rufangura, P.; Sabah, C. Graphene-based wideband metamaterial absorber for solar cells application. *J. Nanophotonics* **2017**, *11*, 036008. [CrossRef]
22. Cen, C.; Chen, Z.; Xu, D.; Jiang, L.; Chen, X.; Yi, Z.; Wu, P.; Li, G.; Yi, Y. High quality factor, high sensitivity metamaterial graphene—Perfect absorber based on critical coupling theory and impedance matching. *Nanomaterials* **2020**, *10*, 95. [CrossRef] [PubMed]
23. Patel, S.K.; Charola, S.; Jani, C.; Ladumor, M.; Parmar, J.; Guo, T. Graphene-based highly efficient and broadband solar absorber. *Opt. Mater.* **2019**, *96*, 109330. [CrossRef]
24. Lin, K.T.; Lin, H.; Yang, T.; Jia, B. Structured graphene metamaterial selective absorbers for high efficiency and omnidirectional solar thermal energy conversion. *Nat. Commun.* **2020**, *11*, 1389. [CrossRef] [PubMed]
25. Baqir, M.A.; Choudhury, P.K.; Akhtar, M.N. ZrN fractal-graphene-based metamaterial absorber in the visible and near-IR regimes. *Optik* **2021**, *237*, 166769. [CrossRef]
26. Alsaif, H.; Patel, S.K.; Ali, N.B.; Armghan, A.; Aliqab, K. Numerical Simulation and Structure Optimization of Multilayer Metamaterial Plus-Shaped Solar Absorber Design Based on Graphene and SiO2 Substrate for Renewable Energy Generation. *Mathematics* **2023**, *11*, 282. [CrossRef]

27. Parmar, J.; Patel, S.K. Tunable and highly sensitive graphene-based biosensor with circle/split ring resonator metasurface for sensing hemoglobin/urine biomolecules. *Phys. B Condens. Matter* **2021**, *624*, 413399. [CrossRef]
28. Jadeja, R.; Charola, S.; Patel, S.K.; Parmar, J.; Ladumor, M.; Nguyen, T.K.; Dhasarathan, V. Numerical investigation of graphene-based efficient and broadband metasurface for terahertz solar absorber. *J. Mater. Sci.* **2020**, *55*, 3462–3469. [CrossRef]
29. Yang, X.S. Nature-inspired optimization algorithms: Challenges and open problems. *J. Comput. Sci.* **2020**, *46*, 101104. [CrossRef]
30. Pornsuwancharoen, N.; Jalil, M.A.; Amiri, I.S.; Ali, J.; Yupapin, P. Dual mode grating sensor using microring conjugate mirror and plasmonic island. *Microw. Opt. Technol. Lett.* **2018**, *60*, 2595–2599. [CrossRef]
31. Kler, A.M.; Zharkov, P.V.; Epishkin, N.O. Parametric optimization of supercritical power plants using gradient methods. *Energy* **2019**, *189*, 116230. [CrossRef]
32. Bağmancı, M.; Karaaslan, M.; Ünal, E.; Akgol, O.; Karadağ, F.; Sabah, C. Broad-band polarization-independent metamaterial absorber for solar energy harvesting applications. *Phys. E Low-Dimens. Syst. Nanostructures* **2017**, *90*, 1–6. [CrossRef]
33. Yu, P.; Chen, X.; Yi, Z.; Tang, Y.; Yang, H.; Zhou, Z.; Duan, T.; Cheng, S.; Zhang, J.; Yi, Y. A numerical research of wideband solar absorber based on refractory metal from visible to near infrared. *Opt. Mater.* **2019**, *97*, 109400. [CrossRef]
34. Patel, S.K.; Charola, S.; Parmar, J.; Ladumor, M.; Ngo, Q.M.; Dhasarathan, V. Broadband and efficient graphene solar absorber using periodical array of C-shaped metasurface. *Opt. Quantum Electron.* **2020**, *52*, 250. [CrossRef]
35. Lin, H.; Sturmberg, B.C.P.; Lin, K.-T.; Yang, Y.; Zheng, X.; Chong, T.K.; de Sterke, C.M.; Jia, B. A 90-nm-thick graphene metamaterial for strong and extremely broadband absorption of unpolarized light. *Nat. Photonics* **2019**, *13*, 270–276. [CrossRef]
36. Yu, P.; Yang, H.; Chen, X.; Yi, Z.; Yao, W.; Chen, J.; Yi, Y.; Wu, P. Ultra-wideband solar absorber based on refractory titanium metal. *Renew. Energy* **2020**, *58*, 227–235. [CrossRef]
37. Azad, A.K.; Kort-Kamp, W.J.M.; Sykora, M.; Weisse-Bernstein, N.R.; Luk, T.S.; Taylor, A.J.; Dalvit, D.A.R.; Chen, H.-T. Metasurface Broadband Solar Absorber. *Sci. Rep.* **2016**, *6*, 20347. [CrossRef]
38. Lakshmiprabha, K.E.; Govindaraju, C.; Mahendran, G. Broadband plus-shaped metasurface absorber based on graphene for visible and ultraviolet regions. *Opt. Quantum Electron.* **2022**, *54*, 774. [CrossRef]
39. Liu, B.; Tang, C.; Chen, J.; Xie, N.; Tang, H.; Zhu, X.; Park, G.-S. Multiband and Broadband Absorption Enhancement of Monolayer Graphene at Optical Frequencies from Multiple Magnetic Dipole Resonances in Metamaterials. *Nanoscale Res. Lett.* **2018**, *13*, 153. [CrossRef]
40. Sang, T.; Gao, J.; Yin, X.; Qi, H.; Wang, L.; Jiao, H. Angle-Insensitive Broadband Absorption Enhancement of Graphene Using a Multi-Grooved Metasurface. *Nanoscale Res. Lett.* **2019**, *14*, 105. [CrossRef]
41. Liu, Y.; Chen, Y.; Li, J.; Hung, T.; Li, J. Study of energy absorption on solar cell using metamaterials. *Sol. Energy* **2012**, *86*, 1586–1599. [CrossRef]
42. Patel, S.K.; Charola, S.; Parmar, J.; Ladumor, M. Broadband metasurface solar absorber in the visible and near-infrared region. *Mater. Res. Express* **2019**, *6*, 086213. [CrossRef]
43. Katrodiya, D.; Jani, C.; Sorathiya, V.; Patel, S.K. Metasurface based broadband solar absorber. *Opt. Mater.* **2019**, *89*, 34–41. [CrossRef]